# Direct Observation of a Preinactivated, Open State in BK Channels with β2 Subunits

G. Richard Benzinger, Xiao-Ming Xia, and Christopher J. Lingle

Department of Anesthesiology, Washington University School of Medicine, St. Louis, MO 63110

Proteins arising from the *Slo* family assemble into homotetramers to form functional large-conductance, $Ca^{2+}$- and voltage-activated $K^+$ channels, or BK channels. These channels are also found in association with accessory β subunits, which modulate several aspects of channel gating and expression. Coexpression with either of two such subunits, β2 or β3b, confers time-dependent inactivation onto BK currents. mSlo1+β3b channels display inactivation that is very rapid but incomplete. Previous studies involving macroscopic recordings from these channels have argued for the existence of a second, short-lived conducting state in rapid equilibrium with the nonconducting, inactivated conformation. This state has been termed "pre-inactivated," or O*. β2-mediated inactivation, in contrast, occurs more slowly but is virtually complete at steady state. Here we demonstrate, using both macroscopic and single channel current recordings, that a preinactivated state is also a property of mSlo1+β2 channels. Detection of this state is enhanced by a mutation (W4E) within the initial β2 $NH_2$-terminal segment critical for inactivation. This mutation increases the rate of recovery to the preinactivated open state, yielding macroscopic inactivation properties qualitatively more similar to those of β3b. Furthermore, short-lived openings corresponding to entry into the preinactivated state can be observed directly with single-channel recording. By examining the initial openings after depolarization of a channel containing β2-W4E, we show that channels can arrive directly at the preinactivated state without passing through the usual long-lived open conformation. This final result suggests that channel opening and inactivation are at least partly separable in this channel. Mechanistically, the preinactivated and inactivated conformations may correspond to binding of the β subunit $NH_2$ terminus in the vicinity of the cytoplasmic pore mouth, followed by definitive movement of the $NH_2$ terminus into a position of occlusion within the ion-conducting pathway.

## INTRODUCTION

Rapid inactivation of voltage-dependent $K^+$ channels involves occlusion of the cytoplasmic mouth of the permeation pathway with a tethered peptide. These peptides are either integral to the pore-forming subunit (Hoshi et al., 1990; Zagotta et al., 1990) or portions of associated accessory β subunits (Rettig et al., 1994; Heinemann et al., 1996; Xia et al., 1999, 2003). Inactivation provides a mechanism by which channel activity is self-limited under conditions that would otherwise lead to continuing ion conduction. A characteristic of simple models of pore occlusion is that inactivation is obligatorily coupled to opening of the channel's conduction pathway. However, there are indications of greater complexity in the inactivation of BK-type channels (Solaro et al., 1997; Lingle et al., 2001). In these cases, evidence suggests that the inactivation process is not well described by first-order association of an inactivating peptide with an open channel. Rather, the binding comprises multiple steps (Lingle et al., 2001), and the coupling of inactivation with opening may not be obligatory (Solaro et al., 1997). Here we investigate these properties further.

For BK-type potassium channels, expression of tetramers of the primary α subunit produces functional channels that do not inactivate. Inactivation is conferred by the presence of either of two accessory subunits. In channels incorporating the β2 subunit, inactivation requires an intact triplet of three hydrophobic amino acids, Phe-Ile-Trp (FIW), at the beginning of the β2 $NH_2$ terminus (Xia et al., 2003). In channels incorporating the β3b subunit, inactivation also requires an intact $NH_2$-terminal cytoplasmic tail in the accessory subunit, but the structural requirements have not yet been further defined (Xia et al., 2000).

Several lines of evidence suggest that inactivation of BK channels has significant differences with that of *Shaker* channels. *Shaker* channels transiently carry current during recovery (Demo and Yellen, 1991), and pore-blocking molecules compete for binding with the inactivation particle (Choi et al., 1991). In contrast, BK channels inactivated by the β2 $NH_2$ terminus can recover without passing through a conducting state, and no competition with pore blockers is observed (Solaro et al., 1997). Taken together, these observations suggest that the *Shaker* inactivation particle binds as a simple open channel blocker, while the BK inactivation domain may bind at a distinct, probably more superficial, site.

Correspondence to Christopher J. Lingle:
clingle@morpheus.wustl.edu

Another distinction between *Shaker* and BK inactivation is that inactivation mediated by the β3b subunit does not occur as a simple, first-order binding of an inactivating particle into the pore. Specifically, properties of whole-cell currents require that channels containing the β3b subunit possess a second, kinetically distinct conducting state that exists in rapid equilibrium with the inactivated conformation (Lingle et al., 2001). The simplest scheme accounting for these observations is shown below, with this additional short-lived conducting state designated O*:

$$C \rightleftharpoons O \rightleftharpoons O^* \rightleftharpoons I \qquad \text{(SCHEME 1)}$$
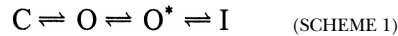
Mechanistically, this two-step inactivation process may represent first the binding of the inactivation particle in the vicinity of the open pore (O→O*) followed by its further movement to occlude the mouth of the conduction pathway (O*→I).

We have speculated that two-step inactivation may be a general feature of both β2- and β3-mediated inactivation, but that differences in the underlying rate constants preclude detection of this process in channels incorporating the β2 subunit (Lingle et al., 2001). It has also been proposed based on structural considerations that *Shaker* and other $K_V$ channels inactivate through a similar multistep path (Zhou et al., 2001; Long et al., 2005). Here we further explore the generality of multistep inactivation. We demonstrate that the β2 subunit also confers a second conducting state and a two-step inactivation process onto BK channels, and we use single channel recordings to visualize this short-lived state directly. A potentially physiologically significant aspect of these results is that channel opening is not absolutely required for the inactivation process to commence, and that channels can initially reach either the open or preinactivated states by kinetically distinct pathways.

Some of these data have been presented previously in abstract form (Benzinger et al., 2005).

## MATERIALS AND METHODS

### Molecular Biology
β subunit constructs were generated by PCR and sequenced to verify that the resultant constructs were generated properly. Constructs were expressed in vitro as cRNA using SP6 RNA polymerase. Details of the construction of the clones used here have been previously described (Xia et al., 1999, 2003).

### Expression in *Xenopus* Oocytes
Expression of the clones used in this report has been previously described (Xia et al., 1999). 1 d after harvest, stage IV *Xenopus* oocytes were injected with 9–36 nl cRNA (10–20 ng/ml). To ensure saturation of expressed channels with β subunits, β subunit message was injected at a 2:1 excess by weight over α subunit cRNA. Previous results have shown that a 1:1 ratio of β2:α subunit mRNA is sufficient to produce saturation of channels with β subunits

(Wang et al., 2002). For single-channel experiments we also used higher ratios (10:1) in some cases.

After injection, oocytes were maintained at 17°C in ND-96 medium (96 mM $Na^+$, 2 mM $K^+$, 1.8 mM $Ca^{2+}$, 1 mM $Mg^{2+}$, 103.6 mM $Cl^-$, 5 mM HEPES, pH 7.5) with the following supplements: 2.5 mM sodium pyruvate, 100 U/ml penicillin, 100 mg/ml streptomycin, 50 mg/ml gentamycin. Oocytes were used 2–14 d after injection.

### Electrophysiology
All currents were recorded in the inside-out patch clamp configuration (Hamill et al., 1981). Pipette resistance was typically 1–3 MΩ. The pipette solution comprised (in mM) 140 K-methanesulfonate, 20 KOH, 2 $MgCl_2$, 10 HEPES, pH 7.2. High resistance seals were formed in a bath solution of ND-96. After development of a seal, the patch was pulled and immediately moved into a local perfusion stream containing (in mM) 140 K-methanesulfonate, 20 KOH, 10 HEPES, 5 HEDTA, pH 7.0. Ca-methanesulfonate was added to achieve a free $Ca^{2+}$ concentration of 10 μM. Free $[Ca^{2+}]$ was verified through use of a $Ca^{2+}$-sensitive microelectrode (Thermo Electron) and comparison to standard solutions (WPI) as previously described (Xia et al., 1999). For experiments involving treatment with cytoplasmic trypsin, trypsin (Sigma-Aldrich) at 1 mg/ml was added to the bath perfusate until modification of current morphology reached steady state, usually 3–5 min.

Currents were recorded using an Axopatch 200B amplifier and pClamp 9.2 software (Molecular Devices). Currents were filtered at 10 kHz through a 4-pole Bessel filter and digitized through a 16-bit DAC at 100 kHz. For macroscopic recordings, five instances of each voltage protocol were averaged and the results recorded. All experiments were performed at room temperature.

### Data Analysis
Whole-cell recordings were analyzed using locally written software running under Scilab 3.0 (Scilab Consortium). Traces were usually analyzed without offline capacitance subtraction. However, for calculation of instantaneous current–voltage relations, the trace resulting from a step to a tail voltage of 0 mV was scaled appropriately and subtracted from the other sweeps in each recording.

Single-channel recordings were first baseline and capacitance corrected visually by subtracting a multicomponent decaying exponential. Corrected traces were interpolated 10-fold by a cubic spline procedure and idealized using a half-amplitude threshold criterion under pClamp 9.2, with idealizations verified visually. Approximately 1% of sweeps contained noticeable excursions to subconductance states; these sweeps were excluded from further analysis. Secondary analysis of the resulting events list was performed using locally written software. Simulated single-channel and macroscopic currents were generated from Markov schemes using the simulation functions of the QuB software package (State University of New York at Buffalo).

Rare reopening events in wild-type mSlo1+β2 channels were analyzed using multichannel patches. In these cases, occasional overlapping reopenings were present. Because lengthy reopenings were rare, these overlaps almost always comprised a short, flickery event superimposed on a more lengthy reopening. Accordingly, the closure that terminated the excursion to the doubly open level was assigned to the opening event immediately preceding it.

## RESULTS

### Kinetic Comparison of β2 and β3b Subunits
Consistent with previous results (Lingle et al., 2001), BK channels incorporating the mSlo1 and β3b subunits displayed rapid, time-dependent but incomplete inactivation, with significant steady-state current remaining even in

the face of lengthy depolarizations (Fig. 1 A). The relative amplitudes of peak, steady-state, and tail currents changed as a function of potential (Fig. 1 B) (and see Uebele et al., 2000; Xia et al., 2000). The complex shape of the peak conductance–voltage relation has been observed previously, and is thought to be due to differing voltage dependences of the activation and inactivation processes (Xia et al., 2000). In contrast, channels incorporating the β2 subunit inactivated somewhat more slowly, but virtually completely, with little steady-state or tail current (Fig. 1, C and D) (and see Xia et al., 1999).

We hypothesized that β2 inactivation might include a two-step inactivation mechanism similar to β3b, but



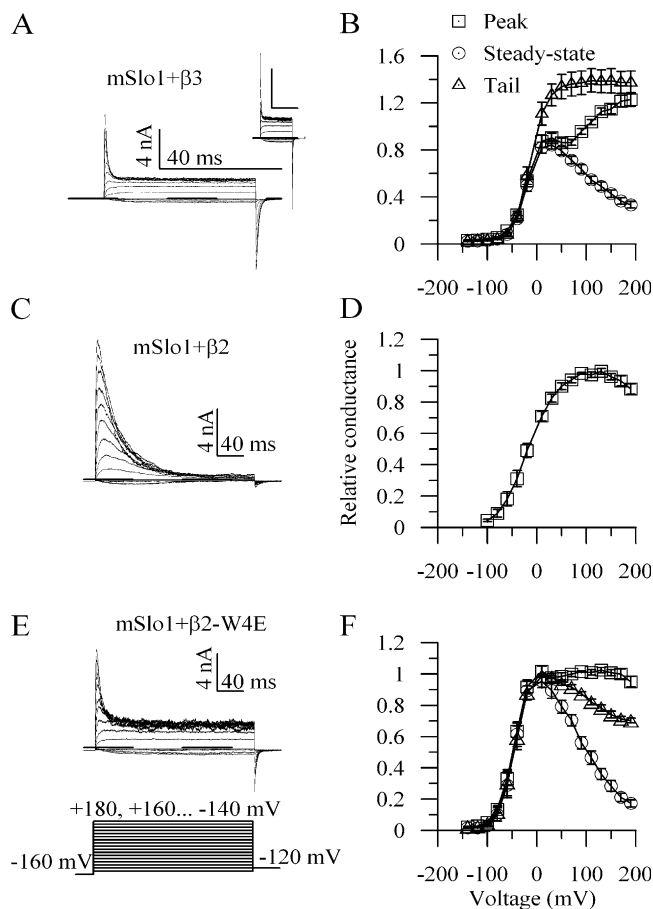**Figure 1.** The W4E mutation renders β2-mediated BK current inactivation properties similar to those of β3b. (A) Currents from a patch expressing mSlo1+β3b channels in response to a family of depolarizations. Inset shows the same currents on a time scale equivalent to C and E. (B) Normalized conductance data from mSlo1+β3b channels. Peak (□), steady-state (○), and tail (△) currents were measured. Peak currents ≤40 mV were fit with a Boltzmann equation, and all current values were normalized to the positive asymptote of this fit ($n = 8$). (C) Current arising from a patch expressing mSlo1+β2 channels. (D) Normalized peak conductance data from mSlo1+β2. ($n = 11$) (E) Current arising from a patch expressing mSlo1+β2-W4E channels. (F) Normalized peak, steady-state, and tail current values calculated as for B ($n = 10$).

that quantitative differences between rate constants might preclude simple detection of a preinactivated state with macroscopic current recordings. A number of mutations in the critical hydrophobic inactivation epitope in the initial segment of the β2 $NH_2$ terminus produce incomplete inactivation (Xia et al., 2003), and may therefore favor easier detection of a putative preinactivated state. Among these, we have focused on β2-W4E because its properties seemed particularly amenable to elucidation of aspects of the proposed two-step inactivation mechanism.

Coexpression of the mutant β2-W4E subunit with mSlo1 α subunit produced channels with incomplete inactivation and large steady-state currents, as well as substantial tail currents upon repolarization (Fig. 1, E and F). Current decay was also somewhat faster in the mutant subunit. At +80 mV, decays were well described by a single exponential fit with τ = 35.5 ± 2.8 ms for β2 ($n = 11$) and τ = 19.0 ± 3.5 ms for β2-W4E ($n = 10$).

The behaviors of α+β2-W4E currents are qualitatively similar to those observed with the β3b subunit, although the inactivation rate of β3b substantially exceeded that of the wild-type and W4E β2 subunits. Furthermore, for both β3b and β2-W4E, the tail upon repolarization had conductances that substantially exceeded the steady-state conductance measured at the conclusion of depolarization (in Fig. 1, B and F, compare triangles with circles).

### Inactivation of α+β2-W4E Channels Exhibits Kinetics Inconsistent with Simple Open-channel Block

We investigated this rapid augmentation of tail current conductance further in Fig. 2. For many gating processes, it is assumed that the rate constants involved in channel gating are slow compared with the rate at which amplifiers can change command potential. Under this assumption, the number of open channels should remain constant over a voltage step, and the current present immediately before and after the step should scale as a simple function of the driving force. Wild-type mSlo1+β2 channels display this approximately ohmic scaling, regardless of whether the duration of the depolarizing prepulse is short or long (Fig. 2 A). Similarly, mSlo1+β2-W4E channels displayed approximately ohmic tail currents if the depolarizingprepulse preceding the voltage step was short and produced little inactivation (Fig. 2 B, black trace). However, when substantial inactivation was allowed to develop before returning to a negative command potential, the current present in the tail reflected an approximately twofold increase in conductance at the earliest measurable time point (Fig. 2 B, star). This augmentation must represent very rapid recovery of channels into a conducting state (summarized in Fig. 2 C).

Channels that have recovered through this rapid mechanism are then susceptible to equally rapid redevelopment of inactivation. mSlo1+β2-W4E channels
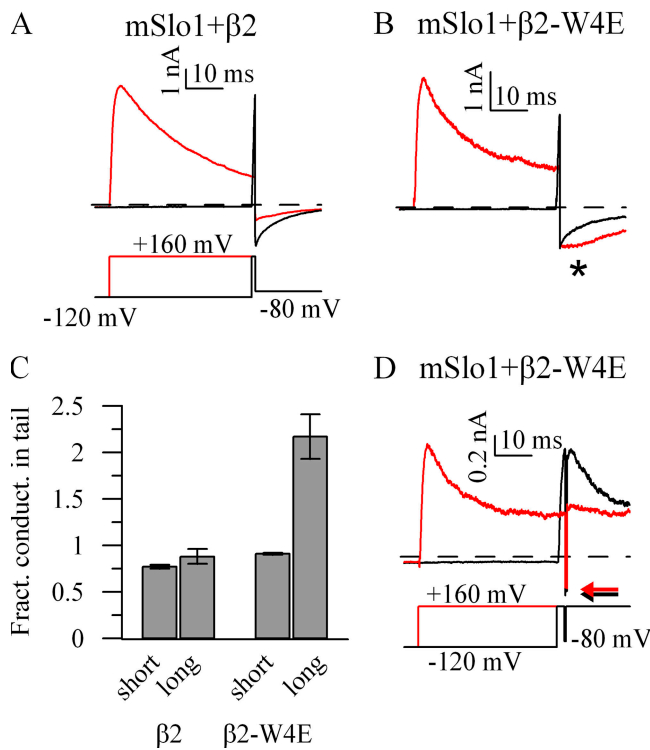
**Figure 2.** β2-W4E channels redistribute extremely rapidly between inactive and conducting conformations. Channels expressing mSlo1+β2 (A) or mSlo1+β2-W4E (B) were depolarized for 1 ms (black) or 40 ms (red) and allowed to recover as shown. After 40-ms depolarizations, mSlo1+β2-W4E displayed an approximately twofold increase in conductance associated with repolarization (*). (C) Fractional change in instantaneous tail current conductance at −80 mV compared with conductance at +160 mV, immediately before repolarization (β2, $n = 6$; β2-W4E, $n = 3$; error bars, ±SEM). (D) A patch expressing mSlo1+β2-W4E was subjected to the indicated voltage protocol. Again, tail current conductance is increased immediately after a long depolarizing prepulse; arrows indicate the instantaneous tail current value during the brief repolarization. This increase is reversed immediately after the onset of a second depolarizing pulse.



**Figure 3.** Inactivation of β2-W4E is associated with biphasic tail currents. (A) mSlo1+β2-W4E tail currents at 40 mV increments, after a 200-ms depolarization as shown. (B) mSlo1+β2-W4E tail currents at 40-mV increments, after a 5-ms depolarization as shown. Insets show tail currents on an expanded time base. (C) Time constants of exponential fits to tail currents from mSlo1+β2-W4E. Tail currents after short depolarizations were fit with single exponentials, and tail currents after long depolarizations were fit with the sums of two exponentials. ○, decaying phase after long depolarization; □, rising phase after long depolarization; △, decaying phase after short depolarization ($n = 4$).

were allowed to inactivate at +160 mV, subjected to a brief (0.5 ms) repolarizing pulse to −80 mV, and then returned to +160 mV (Fig. 2 D). Under this protocol, the tail current present after a lengthy prepulse again displays the nonohmic increase in conductance. During the second depolarization, however, the conductance seen during the tail current undergoes a compensatory immediate, nonohmic decrease and returns to a value close to that before the brief repolarization. This behavior is similar to that seen with the β3b subunit (Lingle et al., 2001).

Both the nearly instantaneous recovery and the equally rapid redevelopment of inactivation occur at rates far in excess of inactivation and recovery rates assayed through traditional paired-pulse protocols in these channels (Xia et al., 2003). This nonohmic behavior is consistent with a very rapid, voltage-dependent equilibration of the inactivated state with a second conducting conformation
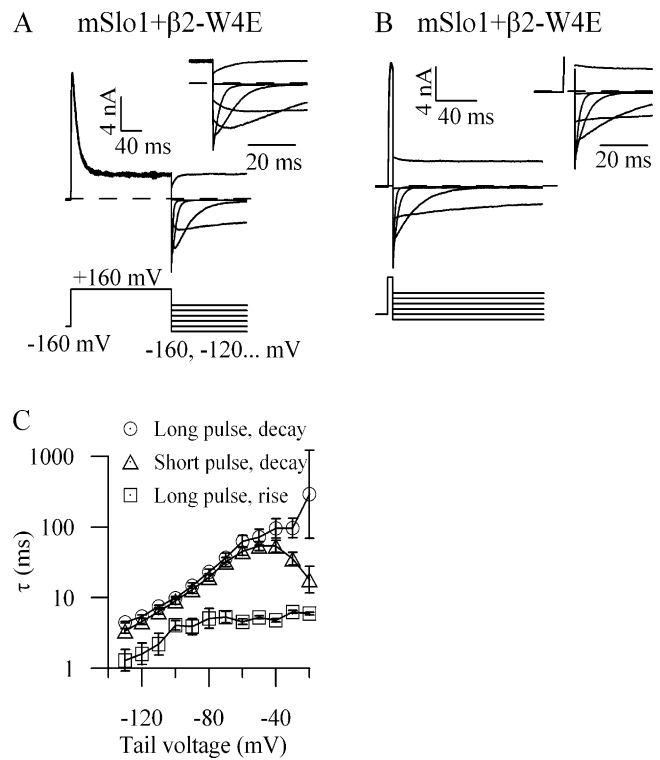
that is distinct from the "classical" open state from which macroscopic inactivation proceeds.

At some voltages, tail currents of inactivated channels were also distinguished by a secondary unblocking component. After a lengthy depolarization that produced steady-state inactivation, recovery to moderately negative voltages (−130 to −20 mV) yielded tail currents with, in addition to the initial nonohmic enhancement, a secondary rising phase (Fig. 3 A). These tail currents were well fit by the sum of a rising and decaying exponential (Fig. 3 C). At a voltage of −80 mV, the potential used for the tail currents in Fig. 2, this rising phase had an apparent time constant of 5.1 ms (3.7–7.0 ms), which was too slow to account for the very rapid increase in tail current conductance noted above. Tail currents after a depolarization too short to produce substantial inactivation produced no such rising phase (Fig. 3 B). These currents were well fit with single exponentials, and they had time courses similar to the decaying phases of tail currents after long depolarizations.
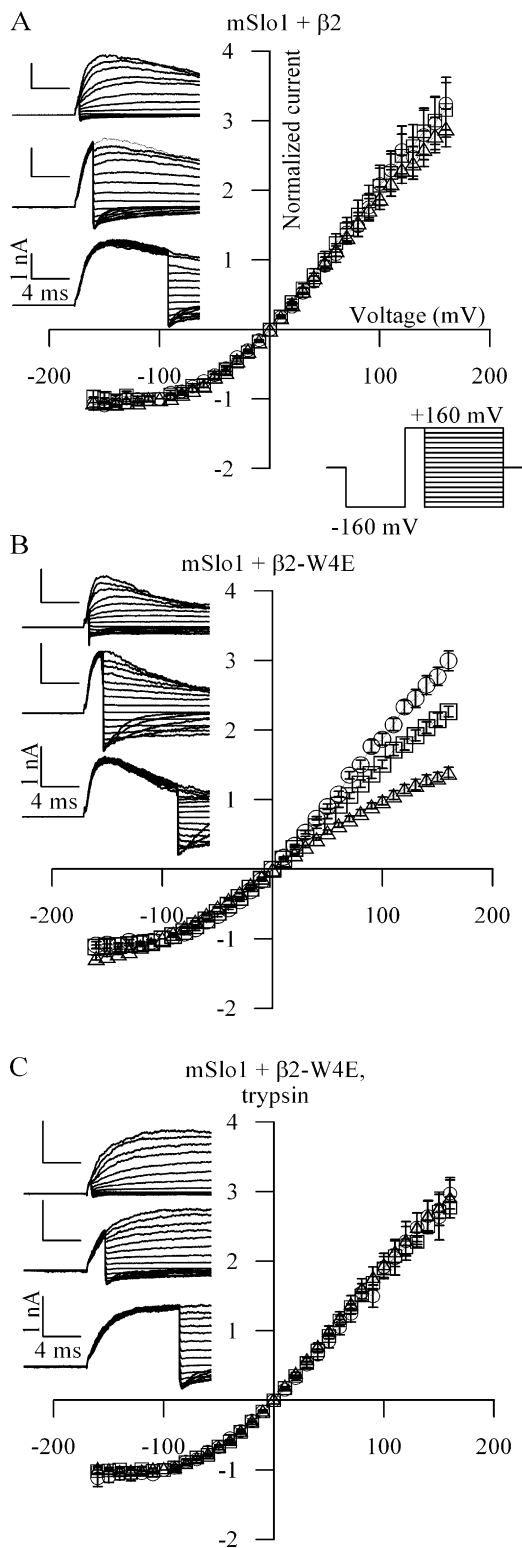
The recovery process evident in these tail currents therefore contains at least three components: an instantaneous recovery, a secondary unblocking, and a final deactivating, closing transition. This behavior is predicted by a model incorporating two open states, such as Scheme 1. It is inconsistent, however, with simplified models containing only one conducting state and one inactivated state.

## Properties of Instantaneous I/V Relations Require an Inactivation-dependent Second Open State

In any Markovian model with voltage-dependent parameters, the relative occupancy of the model's states after a voltage transition will change with time. In the case of Scheme 1, after the initial entry of channels into O, the ratio of occupancy of O and O* will change with time. Because O*, but not O, is assumed to be in a rapid, voltage-dependent equilibrium with the nonconducting I state, the instantaneous current–voltage relation is predicted to change as a function of the relative occupancies of O and O*. Therefore, the instantaneous I/V relation should change as a function of the duration of the depolarization preceding the voltage transition. In contrast, models incorporating only a single conducting state should have instantaneous I/V relations that do not vary with the duration of the prepulse.

Such a time dependence in the instantaneous I/V relation has already been observed in β3b-mediated inactivation (Lingle et al., 2001). Although the instantaneous I/V curve for wild-type mSlo1+β2 is relatively insensitive to prepulse duration (Fig. 4 A), channels incorporating β2-W4E show a strong time dependence to their instantaneous I/V relations (Fig. 4 B). Application of trypsin to the cytoplasmic face of inactivating BK channels is known to eliminate inactivation (Solaro and Lingle, 1992). Accordingly, treatment of mSlo1+β2-W4E patches with cytoplasmic trypsin produced noninactivating currents. Instantaneous I/V relationships for these patches were invariant with the duration of the depolarizing prepulse (Fig. 4 C). The occurrence of a second conducting state is therefore dependent on an intact inactivation pathway. The time dependence of the instantaneous I/V relation and its sensitivity to trypsin together require the presence of a second conducting state and are inconsistent with a model of inactivation based on simple open-channel blockade.

**Figure 4.** Instantaneous current–voltage relationships change with activation step duration. This change requires that channels occupy multiple distinct open states, one of which is in rapid equilibrium with an inactivated state. (A) Patches expressing mSlo1+β2 channels were activated with the indicated voltage protocol, with a depolarizing prepulse lasting 0.5 ms (top traces), 2 ms (middle traces), and 10 ms (bottom traces). For display purposes, raw currents are shown at 20-mV increments. Current was measured 120 μs after the onset of the voltage step from the prepulse potential, after settling of the capacitance transient. For each protocol, these currents were normalized to the value recorded at −100 mV and plotted as follows: ○, 0.5 ms; □, 2 ms; △, 10 ms (n = 6). (B) Patches expressing mSlo1+β2-W4E were recorded as in A (n = 7). (C) Patches expressing mSlo1+β2-W4E were treated with trypsin (1 mg/ml) at the cytoplasmic face until modification of macroscopic current was complete. Trypsin-modified patches were then recorded as above (n = 4).
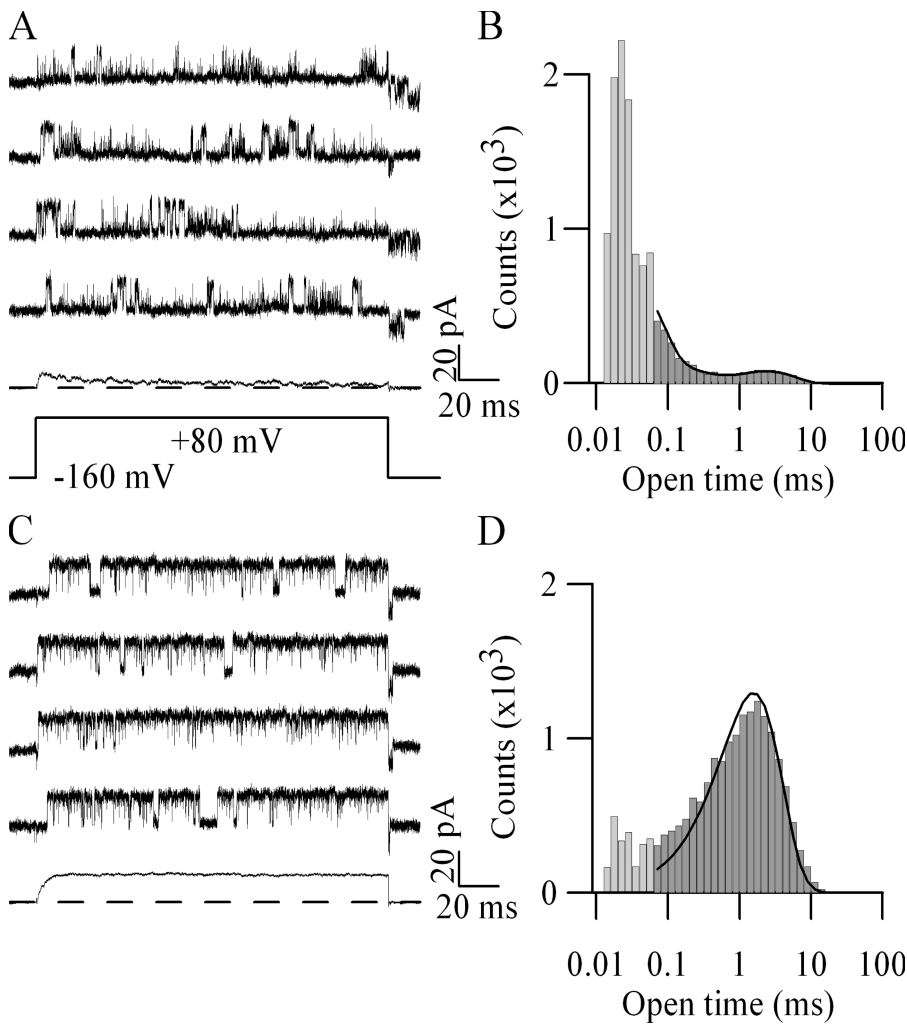
**Figure 5.** mSlo1+β2-W4E channels exhibit short reopenings with characteristics expected for the preinactivated O* state. (A) Recordings from a patch containing one mSlo1+β2-W4E channel using the voltage protocol shown. Bottom trace shows an ensemble average of 40 consecutive sweeps. (B) Histogram of open-time durations from this patch, with bins distributed logarithmically. At event durations less than twice the filter rise time ($2T_r = 66$ µs), significant numbers of events are missed during a half-amplitude idealization. Bins corresponding to this range of times are therefore underestimates and are shown in lighter gray. Line is a three-term exponential fit to these data, with $\tau_{slow} = 2.3$ ms. (C) Recordings from the same patch after treatment with trypsin (1 mg/ml × 2 min) to the intracellular face. Bottom trace shows an ensemble average of 100 consecutive sweeps. (D) Histogram of open-time durations after trypsin treatment, with bins distributed logarithmically. Shading as in B. Line is a one-term exponential fit to these data, with $\tau = 1.6$ ms.

## Single-channel Recordings Exhibit both Long-lived and Inactivation-dependent Short-lived Openings

The state diagram outlined in Scheme 1, along with the macroscopic data presented above, make specific predictions about the single-channel gating behavior of mSlo1+β2-W4E. The high level of steady-state current upon depolarization suggests that channels should show persistent reopenings during a pulse. These openings should fall into two distinct categories: very brief events comprising recovery only to the preinactivated state followed by reinactivation (I→O*→I), and longer openings comprising more rare recovery into the longer-lived, classical conducting state (I→[O*→O]→I).

Recordings from patches containing single mSlo1+β2-W4E channels display this behavior (Fig. 5 A). Periods of numerous, poorly resolved flickery openings are interspersed with occasional longer excursions to the conducting state. Idealization of these data and construction of open-time histograms bear out this qualitative observation (Fig. 5 B). Open-time histograms have two very distinct primary components: a high-amplitude compo-

nent comprising openings usually lasting <100 µs, and a smaller component of distinct, more lengthy openings typically lasting >1 ms.

The presence of a two-component open-time histogram requires a scheme with at least two conducting states. We believe that these two states are kinetically adjacent, and that the O* state is an inactivation-dependent, conducting state that can be accessed by recovery from the inactivated conformation. In principle, one can also construct a scheme in which the short-lived open state represents a "branch" of the activation pathway, and is not itself a function of inactivation. One such scheme is shown below:

$$
\begin{array}{c}
O^* \\
\Updownarrow \\
C \rightleftharpoons O \rightleftharpoons I
\end{array}
\qquad \text{(SCHEME 2)}
$$
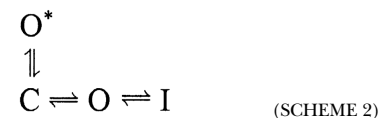
To distinguish between these two possibilities, we removed inactivation from single-channel patches by treatment with trypsin. Treated patches showed an
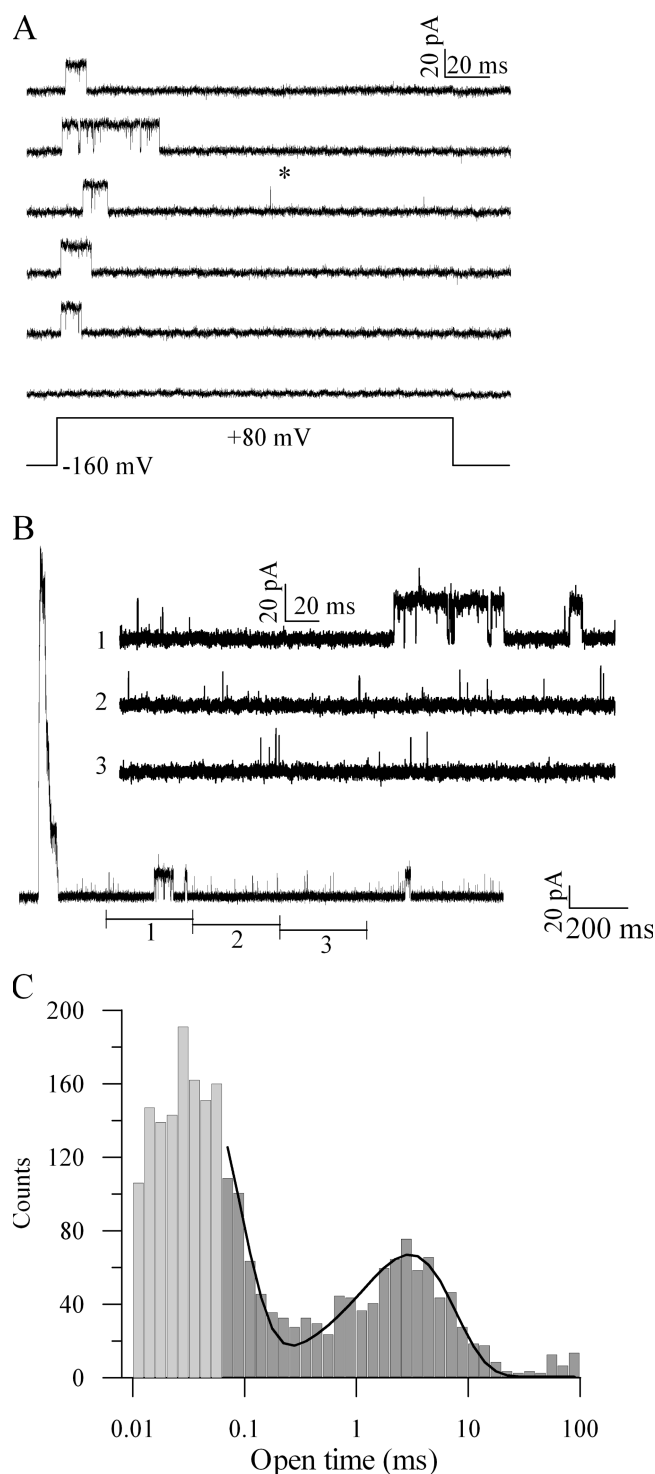
**Figure 6.** Wild-type channels undergo occasional short-lived reopenings. (A) Recordings from a patch containing one mSlo1+β2 channel using the voltage protocol shown. A single brief reopening is shown (*). (B) Recording from a patch containing at least 15 mSlo1+β2 channels during a lengthy depolarization to +80 mV. Insets 1–3 show segments of this trace on an expanded baseline. (C) Histogram of open-time durations from this patch, with bins distributed logarithmically. Events less than twice the filter rise time ($2T_r = 66$ μs) are shown in lighter gray. Line shows a fit to the data with a double exponential decay. Only events >$2T_r$ were included in the fit. $\tau_{slow} = 3.0$ ms.

almost-complete absence of short-lived openings, displaying instead only openings with durations similar to the longer-lived events before trypsin treatment (Fig. 5, C and D). The presence of short-lived openings therefore requires the presence of an intact inactivation pathway, consistent with the idea that the short-lived openings represent a preinactivated state, as depicted in Scheme 1.

Occasionally, these patches also displayed lengthy quiescent states. (see, e.g., the last trace in Fig. 5 C.) These states were usually substantially longer than the latency before initial opening upon depolarization. It is therefore likely that this behavior represents an occasional, long-lived nonconducting state that is not described by any of the schemes considered here.

It is possible that the occurrence of an inactivation-dependent open state in mSlo1+β2-W4E represents a phenomenon unique to this particular mutant and is not characteristic of the wild-type β2 subunit. To answer this concern, we looked for the presence of similar short and long reopenings in wild-type mSlo1+β2 channels. In macroscopic recordings, wild-type channels have little persistent current. Accordingly, recordings from patches containing single mSlo1+β2 channels displayed reopenings very rarely. Occasionally, however, single brief, flickery reopenings were evident (Fig. 6 A). To view more of these events, we recorded prolonged depolarizations from patches containing 10–20 wild-type channels (Fig. 6 B). These recordings showed both frequent brief openings and uncommon longer openings. An open-time histogram constructed from idealized data revealed a bimodal distribution very similar to that associated with β2-W4E (Fig. 6 C). The mean open time for the longer openings was $2.3 \pm 0.5$ ms ($n = 3$). Therefore, the wild-type β2 subunit confers a preinactivated state onto BK channels in a manner similar to that of the W4E mutant.

### Channels Arrive at the O and O* States by Different Paths

A strictly linear sequential model like that presented in Scheme 1 predicts that initial openings in response to depolarization should always traverse both conducting states. Consequently, the first opening in each sweep should be, on average, long-lived. In wild-type mSlo1+β2, this prediction usually holds true. In only $2.0 \pm 0.5\%$ of sweeps (in excess of those predicted by the tail of the longer open-time distribution, $n = 3$ patches) does the initial opening last for <0.2 ms, while considerably more than half of reopenings are short-lived (see Fig. 6 C).

However, for mSlo1+β2-W4E channels, the simple expectation of Scheme I does not hold. For example, the top sweep in Fig. 5 A shows an apparent initial opening that is very short lived. Even for Scheme I, very short initial openings would be occasionally expected as a matter of chance. To assess whether these short-lived
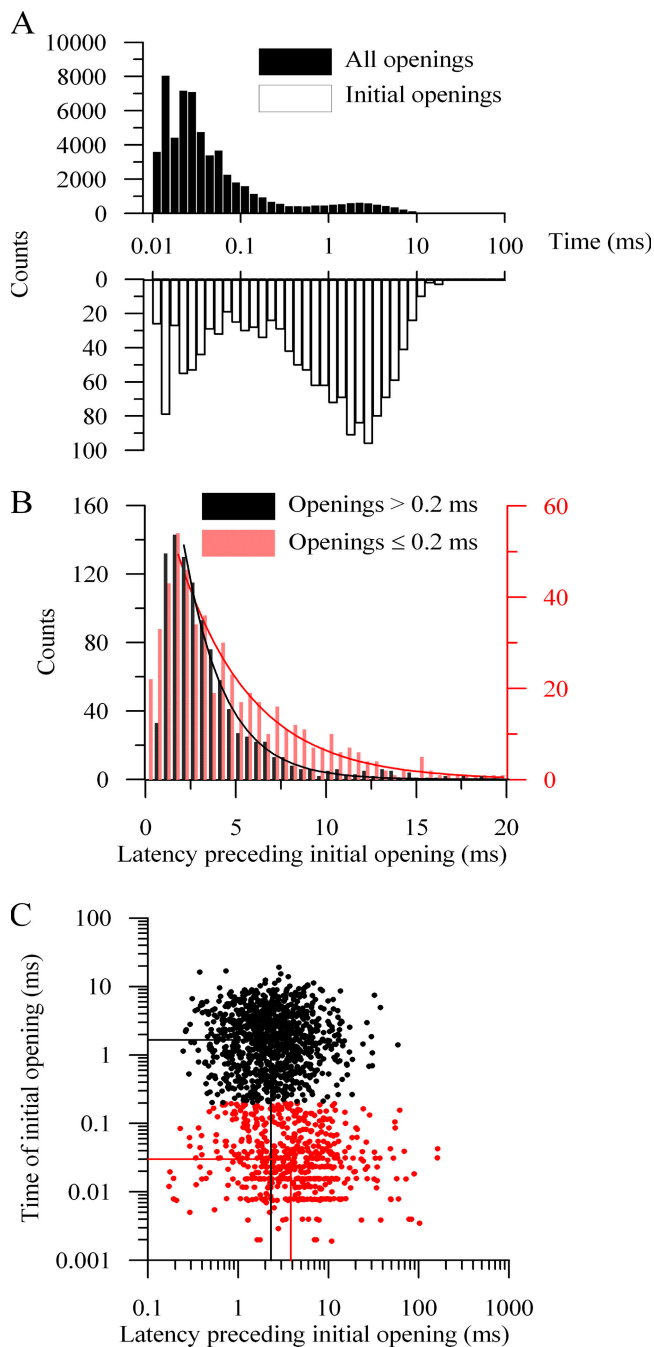
**Figure 7.** Channels arrive at initial long- and short-lived openings by different kinetic paths. (A) Histograms of open-time duration for all openings (solid bars) and initial openings (open bars) of a single mSlo1+β2-W4E channel after depolarizations to +80 mV. Bins are spaced logarithmically. (B) Histograms of the latency before initial opening, binned linearly and segregated by the duration of this first opening. Initial openings were categorized into two groups, those lasting >0.2 ms and those <0.2 ms, based on the nadir between the two components of the open-time histograms shown in A. Lines show single-exponential fits to the decaying phases of the latency histograms (latencies ≥2 ms). For openings >0.2 ms (black), τ = 2.2 ms; for openings ≤0.2 ms (red), τ = 4.0 ms. (C) Scatterplot displaying the durations of initial openings versus the durations of the latency before opening. Events were again segregated as "short" (red) or "long" (black) by a criterion of 0.2 ms. Lines show the average duration and latency (computed

initial openings occur more frequently than predicted, we compared an open-time histogram derived from all openings with one derived from only the initial opening in each depolarization (Fig. 7 A). Although the initial openings were significantly enriched in long-lasting events, the distribution of these openings remained significantly bimodal, indicating that, on average, α + β2-W4E channels open to the short-duration, preinactivated state ∼39 ± 3% of the time (n = 4 patches). These channels are therefore readily able to pass directly to the preinactivated state without visiting the classical open conformation.

Because channels can enter into either the open or preinactivated states directly, the different kinetic paths that lead to those two types of openings may produce differing latencies preceding the initial conducting event. To assess this possibility, we chose 200 μs, the local minimum between the two components of the open-time histograms, as a criterion for separating short and long openings. We compiled histograms of the latency preceding first opening separately for short and long events (Fig. 7 B). Fitting the decaying portions of these histograms with single exponentials showed a longer average latency preceding short openings than that preceding long openings. For long openings, $\tau_{lat}$ = 2.1 ± 0.5 ms; for short openings, $\tau_{lat}$ = 4.3 ± 1.1 ms (n = 4).

To illustrate this difference more directly, we constructed a scatter plot of the durations of the first latency and the initial opening for each sweep in a patch (Fig. 7 C). Openings were again separated as >200 μs (black) or ≤200 μs (red). These distributions were log-transformed and averaged. The difference in latency for short events vs. long events when averaged in this manner, 3.9 vs. 2.3 ms in this example, was not large but was highly statistically significant (P < 0.0001, Student's t test). Data from four similar patches yielded an average latency preceding short events of 3.4 ms (2.9–4.0, mean ± SEM), and for long events of 1.9 ms (1.5–2.4, mean ± SEM). We therefore conclude that, for α+β2-W4E channels, the path toward inactivation cannot be represented by a purely linear sequential model, and that channels may pass through different pathways before initially opening to the O or O* states.

## DISCUSSION

Here we have shown that BK channels incorporating the β2 accessory subunit possess two kinetically distinct conducting states, one of which is uniquely associated

logarithmically) for each population. For long events, the average latency was 2.31 ms (mean ± SEM, 2.25–2.38 ms, n = 1022). For short events, the average latency was 3.86 ms (mean ± SEM, 3.68–4.05 ms, n = 558).

with inactivation. In addition to the long-lived open state characteristic of noninactivating BK channels, channels can enter a very short-lived conducting conformation that is in rapid, voltage-dependent equilibrium with the inactivated state. Specific mutations of the $NH_2$ terminus of the β2 subunit, by altering the kinetics of the inactivation process, produce incomplete inactivation and facilitate detection of this state.

Both macroscopic and single-channel data provide evidence for the existence of this state. Channels including mutant β2 subunits display apparent nonohmic increases in tail current, consistent with redistribution between I and O*, and instantaneous current–voltage relationships differ with the relative proportions of channels in the O and O* states. Both brief reopenings (to O*) and lengthy reopenings (to O* and O) are visible in single-channel recordings from both wild-type and mutant channels. Finally, enzymatic treatment to remove inactivation removes the preinactivated state.

### Structural Correlates of the Preinactivated State

The simplest structural explanation consistent with these observations is that the β2 $NH_2$ terminus produces inactivation through a multistep blocking process. In this model, the preinactivating transition corresponds to the binding of the $NH_2$ terminus in close association with the pore, while full inactivation occurs when the $NH_2$ terminus moves further and occludes it. The location of the initial binding site remains unknown. However, the short duration of openings to the preinactivated state suggests that the site must be close to the final binding site for full inactivation.

Is this model consistent with the structural features of the BK channel cytoplasmic face? Recent structural work with $K_V$ channels has suggested that the *Shaker* inactivation domains reach the ion-conducting pore through lateral "side portals" in the cytoplasmic portion of the channel (Gulbis et al., 2000; Long et al., 2005). BK channels also possess large cytoplasmic domains tethered to the cytoplasmic end of the S6 helix. It therefore seems likely that access of the BK inactivation particle to the conduction pathway occurs through side portals, as well. Mutagenesis experiments with the BK β2 $NH_2$ terminus have shown that many different amino acid sequences between the hydrophobic triplet and the transmembrane region will support inactivation (Xia et al., 2003). In addition, an NMR structure for the $NH_2$ terminus showed considerable flexibility over much of this region (Bentrop et al., 2001). These facts together suggest that the $NH_2$-terminal inactivation domain may be sufficiently pliant to make its way through a postulated side portal.

The limited length of the BK inactivation domain also suggests that it may access the conduction pathway through a side portal. Mutagenesis studies in β2 have shown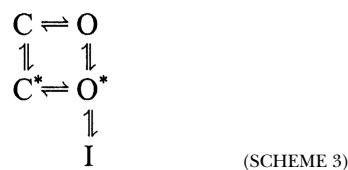 that a linker region of only 12 amino acids be-tween the membrane and the hydrophobic triplet is sufficient to support functional inactivation (Xia et al., 2003). In a maximally extended conformation, this minimally acceptable 15–amino acid linker can extend 57 Å (Creighton, 1993). For comparison, the cytoplasmic "T1" domain of $K_V1.2$ is ∼40 Å in height (Long et al., 2005), and BK α subunits have a cytoplasmic domain that is likely to be considerably larger than that of *Shaker*-type channels (Stuhmer et al., 1989; Butler et al., 1993). Given such a large cytoplasmic region, access to the conduction pathway through a side portal seems very likely.

If the inactivation domain enters the channel in this manner, ample opportunity exists for interaction between the inactivation domain and the α subunit before the pore is occluded. Preinactivation may represent the interaction of the β2 $NH_2$-terminal residues with the lining of the side portal, followed by full inactivation as the $NH_2$ terminus advances into the pore. Alternately, preinactivation may involve the interaction of the hydrophobic triplet within the channel's central axis, but at a more superficial, nonoccluding position than that associated with inactivation. In either case, excursions to the preinactivated state are very short, while the macroscopic rate of channel inactivation is considerably slower. These facts imply that entry from the open state into the preinactivated state is the rate-limiting step in channel inactivation. The β2 $NH_2$ terminus in its preinactivated position therefore must be very close to its inactivating, occlusive conformation. Given the side portal structure of $K_V$ channels, it is perhaps more surprising that *Shaker* inactivation appears to occur as a first-order association process. Further work with *Shaker* may reveal intermediate steps in its inactivation pathway, as well (Zhou et al., 2001).

The proposed movement of the β2 inactivation particle through a side portal raises additional questions related to the stoichiometry of channel inactivation. Previous work using low levels of β2 mRNA has shown that the presence of a single β2 subunit in the channel complex is sufficient to permit inactivation, and that additional β2 subunits increase the rate of inactivation in a dose-dependent manner (Wang et al., 2002). The presence of four side portals and four β2 subunits admits the possibility that multiple β2 $NH_2$ termini can exist in a preinactivated conformation, contained within multiple side portals, simultaneously. Alternately, if the preinactivated conformation involves a degree of impingement into the channel's central axis, it may be that preinactivation is competitive, and that multiple $NH_2$ termini cannot concurrently occupy this state. We believe that these alternatives are potentially experimentally distinguishable.

### Ability of BK Channels to Inactivate without First Opening

Our results indicate that fully closed channels bearing the β2-W4E subunit can occasionally open directly into

the preinactivated state without ever passing through a long-lived open conformation. This observation is incompatible with the strict linear sequential model given in Scheme 1. Previous studies have shown that BK channels need not conduct current during recovery from inactivation, implying that closure of a channel's activation gate is not impeded by the presence of a docked inactivation particle (at least during recovery) (Solaro et al., 1997). This result suggests that even the final binding site of the inactivation particle within the pore is more superficial than that usually envisioned for *Shaker* channels. Therefore, the simplest model explaining these data allows for mSlo1+β2-W4E channels to reach (at least) the preinactivated state before channel opening:

$$
\begin{array}{ccc}
C & \rightleftharpoons & O \\
\Updownarrow & & \Updownarrow \\
C^* & \rightleftharpoons & O^* \\
& & \Updownarrow \\
& & I
\end{array}
$$

(SCHEME 3)

In this model, movement of the inactivation particle into the preinactivated position can precede opening of the activation gate (C→C*→O*), yielding an initial brief opening. Because wild-type mSlo1+β2 channels show very few direct openings to the short-lived O* state, it is natural to ask whether Scheme 3 only applies to the mutated variant that we have studied. Prior studies on native BK channels in adrenal chromaffin cells, which most likely include the β2 subunit, have shown that, under conditions of weak activation, these channels can inactivate without ever opening (Ding and Lingle, 2002). Transition through the classical open state was therefore not an absolute consequence of depolarization in these channels, either.

Is it then possible to account for the empiric differences in single-channel behavior between wild-type and mSlo1+β2-W4E channels upon initial activation within the context of Scheme 3? We are aware of two possibilities. First, wild-type channels may have a slower rate of preinactivation (C→C*) with respect to activation (C→O) than is the case in mSlo1+β2-W4E channels, thereby favoring full openings upon depolarization. In support of this idea, we observed that macroscopic current decay after depolarization was approximately twofold slower at +80 mV for channels including wild-type β2 than for β2-W4E. This result suggests that the preinactivating process is slower in wild-type channels than in channels containing β2-W4E.

Second, it is possible that, despite our hyperpolarizing prepulses, some mSlo1+β2-W4E channels remain inactivated at the beginning of our depolarizations. In contrast, wild-type channels might be fully available by the onset of depolarization. Although we cannot exclude this possibility, we do not consider it likely. In 10 μM Ca²⁺, BK channels incorporating wild-type β2 are virtually fully available at potentials more negative than −120 mV (Ding and Lingle, 2002). Our prepulse occurred at −160 mV, providing a considerable margin of safety. Furthermore, despite the steady-state conductance properties of mSlo1+β2-W4E, very little current is carried by these channels at the end of the hyperpolarizing prepulse, suggesting that few, if any, channels remain open or inactivated at this point (see Fig. 1 C).

We therefore prefer the view that the observed difference in the tendency of wild-type and mSlo1+β2-W4E channels to open directly to the preinactivated state is explicable within Scheme 3. It likely represents a difference in the relative rates of the opening and preinactivating transitions, a difference that is consistent with other known macroscopic data.

To assess the ability of Scheme 3 to explain the observed properties of mSlo1+β2-W4E current, we constructed a quantitative model and assessed the resulting simulated events. The process of BK channel activation encapsulates the movement of up to four voltage sensors and the binding of up to four Ca²⁺ ions and is therefore represented by a Markov scheme comprising many dozens of states (Horrigan and Aldrich, 2002). The rate constants associated with activation are not well constrained by single-channel data obtained at single values of voltage and [Ca²⁺]. For the present purpose, however, at least one additional resting state (denoted $C_R$) was required to adequately model the latency preceding initial channel opening. The resulting six-state model is shown in Fig. 8 A.

To maximally constrain the behavior of this model, we assumed an absence of allosteric coupling between the processes of channel opening and inactivation particle binding. Under this assumption, the model contained eight free parameters. Furthermore, a scheme of this form allowed for direct estimation of all rate constants from aggregate statistics of single-channel behavior (see Table I) and did not require maximum-likelihood estimation of otherwise-unconstrained parameters.

Simulated events resulting from this model accurately recapitulated the behavior of mSlo1+β2-W4E channels (Fig. 8 B). Single-channel openings occurred as either isolated, very brief reopenings or as bursts of longer-lived events. Macroscopic traces showed partial inactivation and a large steady-state standing current, consistent with macroscopic recordings at +80 mV (compare Fig. 8 B, third trace, with Fig. 1 E). "Trypsinization," as represented by removal from the model of all preinactivated and inactivated states, increased the steady-state open probability and eliminated the population of brief, flickery openings (Fig. 8 C).

This model also predicted the ability of channels to open initially into the preinactivated O* state. However, channels followed this path with a rate much lower than the 39% observed experimentally. This discrepancy arises from the interaction of two of the observed kinetic
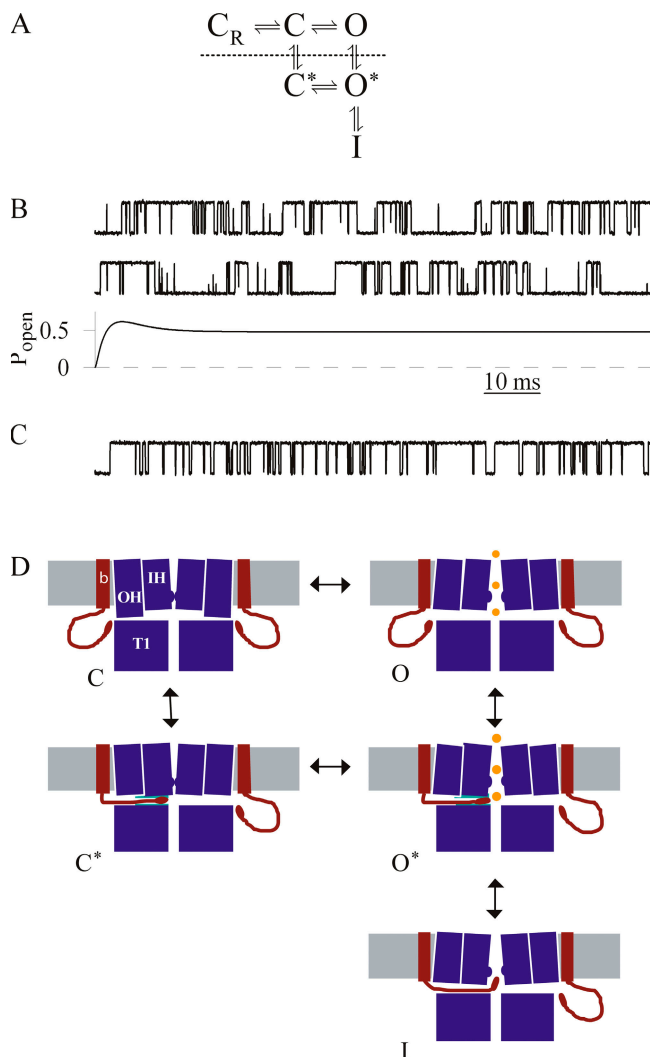
**Figure 8.** Models of preinactivation. (A) A six-state Markov scheme incorporating Scheme 3 with the addition of an extra, nonconducting resting state, $C_R$. In the absence of allosteric coupling, rate constants on opposite sides of the central loop are assumed to be identical (e.g., $k_{C \to C^*} = k_{O \to O^*}$) To simulate removal of inactivation by trypsin, all states below the dotted line were removed. (B) Predictions of the scheme shown in A, with rate constants as listed in Table I. Rate constants were estimated from data acquired at +80 mV and 10 $\mu$M $Ca^{2+}$. Top two traces, simulated single channel data, superimposed on 1 pA RMS noise, digitally lowpass filtered at 10 kHz. Bottom trace, simulated macroscopic current at +80 mV. Dotted line is zero-current level. (C) Simulated single-channel data after removal of inactivation by "trypsin," processed as above. (D) A structural conception of the preinactivated state. Images depict a cartoon showing two opposing $\alpha$ subunits from the mSlo1 tetramer, flanked by two $\beta$2 subunits. The five states shown correspond to those in Scheme 3. $\beta$, $\beta$2 subunit; OH, outer helix bundle (S0–S4); IH, inner helix bundle (S5–S6); T1, channel cytoplasmic domain (see Long et al., 2005). The depolarization-induced change permissive for preinactivation is represented as movement at the cytoplasmic face of the outer helix bundle. Possible locations for the interaction associated with preinactivation are shown in green in the C* and O* states.

parameters. A higher fraction of channels initially opening into O* predicts a higher rate of closed state preinactivation (C→C*), while a longer duration of long-lived bursts predicts a lower rate of open state preinactivation (O→O*). Permitting the presence of (negative) allosteric coupling between channel opening and preinactivation allows for a higher rate of openings into the preinactivated state without limiting the burst length of longer openings. The extent and physical basis of this allostery may prove a fruitful area for further study.

The presence of short-lived initial openings implies that channels can reach the preinactivated state without passing through the classical open conformation. This process might arise either from preinactivation of a fully closed channel or from an initial voltage-dependent conformational change that precedes channel opening and favors preinactivation. Previous studies have shown substantial steady-state levels of inactivation of BK channels incorporating the $\beta$2 subunit at potentials for which activation was minimal (Ding and Lingle, 2002). However, the presence of a closed, fully inactivated state is not necessary to explain the current and previous results. Macroscopic rates of inactivation display only a very modest voltage dependence, despite the obvious voltage dependence of steady-state availability curves (Ding and Lingle, 2002). Further, charged residues are not required on the $\beta$2 $NH_2$ terminus to produce inactivation (Xia et al., 2003). The apparent development of steady-state inactivation in the absence of conductance could therefore reflect channel entry into the closed, preinactivated conformation (C*), followed by full inactivation almost immediately upon channel opening during the test pulse.

An important implication of this idea is that a structural transition associated with activation but preceding channel opening is required to permit movement of the $NH_2$ terminus into its full inactivating position. One possible candidate for this transition is the movement of the S4 voltage sensor. Current evidence suggests that substantial gating charge movement occurs very rapidly upon depolarization and significantly before the onset of channel opening (Horrigan and Aldrich, 1999). Therefore, S4 movement is well poised to act as a permissive switch for channel inactivation by the $\beta$2 $NH_2$ terminus.

A cartoon encapsulating these ideas is shown in Fig. 8 D. In this scheme, a conformational change associated with movement of the voltage sensor is permissive for preinactivation and precedes channel opening. Preinactivation is represented by movement of the $\beta$2 $NH_2$ terminus into a side portal, followed by binding at a position close to the ion conduction pathway. Further movement into the pore then corresponds to complete channel inactivation. By permitting inactivation without first passing through the open state, this multistep inactivation process may help regulate levels of BK current across a

| Rate constant | Value (s$^{-1}$) | Derivation[a] |
|---|---|---|
| $k_{CR \to C}$ | 477 | $k_{CR \to C} \approx$ (first latency preceding long events)$^{-1}$ |
| $k_{C \to CR}$ | 4.8 | $k_{C \to CR} = (0.01) \times k_{CR \to C}$[b] |
| $k_{O \to C}$ | 833 | $k_{O \to C} =$ (MOT of trypsinized channels)$^{-1}$ |
| $k_{C \to O}$ | 4720 | $\dfrac{k_{C \to O}}{k_{C \to O} + k_{O \to C}} =$ (equilibrium $P_O$ in trypsin) [c] |
| $k_{O^* \to I}$ | 24167 | $k_{O^* \to I} + k_{O^* \to C^*} =$ (MOT of short openings)$^{-1}$ [d] |
| $k_{I \to O^*}$ | 625 | $k_{I \to O^*} =$ (long component of closed times)$^{-1}$ |
| $k_{O^* \to O}$ | 5864 | $\left(1 + \dfrac{k_{O^* \to O}}{k_{O^* \to I}}\right)\left(\dfrac{1}{k_{O \to O^*}}\right) =$ MOT of long bursts |
| $k_{O \to O^*}$ | 175 | $\dfrac{k_{O^* \to I} + k_{O^* \to C^*}}{k_{O^* \to I} + k_{O^* \to C^*} + k_{O^* \to O}} = \dfrac{\text{total short reopenings}}{\text{total all reopenings}}$ |

[a]Parameters are calculated from four single-channel patches at +80 mV and 10 μM Ca$^{2+}$.

[b]Because activation is greatly favored at +80 mV, the rate of deactivation is assumed to be small compared to the rate of activation (see Fig. 1 F).

[c]Calculation of this $P_O$ excludes lengthy nonconducting periods, which are assumed to be the result of a slower modal process not represented in this model.

[d]Short openings are assumed to exclude excursions to the full open state O.

[e]The treatment of bursts by Colquhoun and Hawkes (Colquhoun and Hawkes, 1995) assumes a single conducting state. Their relation is applicable to this model under the assumption that the total time spent in O* and in deactivations to C is small compared to the total open time of a burst.

range of voltages in tissues in which inactivating BK accessory subunits are found.

## REFERENCES

Bentrop, D., M. Beyermann, R. Wissmann, and B. Fakler. 2001. NMR structure of the "ball-and-chain" domain of KCNMB2, the β2-subunit of large conductance Ca$^{2+}$- and voltage-activated potassium channels. *J. Biol. Chem.* 276:42116–42121.

Benzinger, G.R., J.P. Ding, X.M. Xia, and C.J. Lingle. 2005. Direct observation of a pre-inactivated open state in BK channels. *Biophys. J.* 88:101a.

Butler, A., S. Tsunoda, D.P. McCobb, A. Wei, and L. Salkoff. 1993. mSlo, a complex mouse gene encoding "maxi" calcium-activated potassium channels. *Science.* 261:221–224.

Choi, K.L., R.W. Aldrich, and G. Yellen. 1991. Tetraethylammonium blockade distinguishes two inactivation mechanisms in voltage-activated K$^+$ channels. *Proc. Natl. Acad. Sci. USA.* 88:5092–5095.

Colquhoun, D., and A.G. Hawkes. 1995. The principles of the stochastic interpretation of ion-channel mechanisms. *In* Single-Channel Recording. B. Sakmann and E. Neher, editors. Plenum Press, New York. 397–479.

Creighton, T.E. 1993. Proteins: Structures and Molecular Properties, Second edition. W.H. Freeman and Company, New York. 507 pp.

Demo, S.D., and G. Yellen. 1991. The inactivation gate of the *Shaker* K$^+$ channel behaves like an open-channel blocker. *Neuron.* 7:743–753.

Ding, J.P., and C.J. Lingle. 2002. Steady-state and closed-state inactivation properties of inactivating BK channels. *Biophys. J.* 82:2448–2465.

Gulbis, J.M., M. Zhou, S. Mann, and R. MacKinnon. 2000. Structure of the cytoplasmic β subunit-T1 assembly of voltage-dependent K$^+$ channels. *Science.* 289:123–127.

Hamill, O.P., A. Marty, E. Neher, B. Sakmann, and F.J. Sigworth. 1981. Improved patch-clamp techniques for high-resolution current recording from cells and cell-free membrane patches. *Pflugers Arch.* 391:85–100.

Heinemann, S.H., J. Rettig, H.R. Graack, and O. Pongs. 1996. Functional characterization of Kv channel β-subunits from rat brain. *J. Physiol.* 493(Pt 3):625–633.

Horrigan, F.T., and R.W. Aldrich. 1999. Allosteric voltage gating of potassium channels II. Mslo channel gating charge movement in the absence of Ca$^{2+}$. *J. Gen. Physiol.* 114:305–336.

Horrigan, F.T., and R.W. Aldrich. 2002. Coupling between voltage sensor activation, Ca$^{2+}$ binding and channel opening in large conductance (BK) potassium channels. *J. Gen. Physiol.* 120:267–305.

Hoshi, T., W.N. Zagotta, and R.W. Aldrich. 1990. Biophysical and molecular mechanisms of *Shaker* potassium channel inactivation. *Science.* 250:533–538.

Lingle, C.J., X.H. Zeng, J.P. Ding, and X.M. Xia. 2001. Inactivation of BK channels mediated by the NH$_2$ terminus of the β3b auxiliary subunit involves a two-step mechanism: possible separation of binding and blockade. *J. Gen. Physiol.* 117:583–606.

Long, S.B., E.B. Campbell, and R. Mackinnon. 2005. Crystal structure of a mammalian voltage-dependent *Shaker* family K$^+$ channel. *Science.* 309:897–903.

Rettig, J., S.H. Heinemann, F. Wunder, C. Lorra, D.N. Parcej, J.O. Dolly, and O. Pongs. 1994. Inactivation properties of voltage-gated K$^+$ channels altered by presence of β-subunit. *Nature.* 369:289–294.

Solaro, C.R., J.P. Ding, Z.W. Li, and C.J. Lingle. 1997. The cytosolic inactivation domains of BKi channels in rat chromaffin cells do not behave like simple, open-channel blockers. *Biophys. J.* 73:819–830.

Solaro, C.R., and C.J. Lingle. 1992. Trypsin-sensitive, rapid inactivation of a calcium-activated potassium channel. *Science.* 257:1694–1698.

Stuhmer, W., J.P. Ruppersberg, K.H. Schroter, B. Sakmann, M. Stocker, K.P. Giese, A. Perschke, A. Baumann, and O. Pongs.

1989. Molecular basis of functional diversity of voltage-gated potassium channels in mammalian brain. *EMBO J.* 8:3235–3244.

Uebele, V.N., A. Lagrutta, T. Wade, D.J. Figueroa, Y. Liu, E. McKenna, C.P. Austin, P.B. Bennett, and R. Swanson. 2000. Cloning and functional expression of two families of β-subunits of the large conductance calcium-activated K+ channel. *J. Biol. Chem.* 275:23211–23218.

Wang, Y.W., J.P. Ding, X.M. Xia, and C.J. Lingle. 2002. Consequences of the stoichiometry of Slo1 α and auxiliary β subunits on functional properties of large-conductance $Ca^{2+}$-activated K+ channels. *J. Neurosci.* 22:1550–1561.

Xia, X.M., J.P. Ding, and C.J. Lingle. 1999. Molecular basis for the inactivation of $Ca^{2+}$- and voltage-dependent BK channels in adrenal chromaffin cells and rat insulinoma tumor cells. *J. Neurosci.* 19:5255–5264.

Xia, X.M., J.P. Ding, and C.J. Lingle. 2003. Inactivation of BK channels by the $NH_2$ terminus of the β2 auxiliary subunit: an essential role of a terminal peptide segment of three hydrophobic residues. *J. Gen. Physiol.* 121:125–148.

Xia, X.M., J.P. Ding, X.H. Zeng, K.L. Duan, and C.J. Lingle. 2000. Rectification and rapid activation at low $Ca^{2+}$ of $Ca^{2+}$-activated, voltage-dependent BK currents: consequences of rapid inactivation by a novel β subunit. *J. Neurosci.* 20:4890–4903.

Zagotta, W.N., T. Hoshi, and R.W. Aldrich. 1990. Restoration of inactivation in mutants of *Shaker* potassium channels by a peptide derived from ShB. *Science.* 250:568–571.

Zhou, M., J.H. Morais-Cabral, S. Mann, and R. MacKinnon. 2001. Potassium channel receptor site for the inactivation gate and quaternary amine inhibitors. *Nature.* 411:657–661.